# Direct Observation of Frictional Contacts: New Insights for State-dependent Properties

JAMES H. DIETERICH[1] and BRIAN D. KILGORE[1]

*Abstract* - Rocks and many other materials display a rather complicated, but characteristic, dependence of friction on sliding history. These effects are well-described by empirical rate- and state-dependent constitutive formulations which have been utilized for analysis of fault slip and earthquake processes. We present a procedure for direct quantitative microscopic observation of frictional contacts during slip. The observations reveal that frictional state dependence represents an increase of contact area with contact age. Transient changes of sliding resistance correlate with changes in contact area and arise from shifts of contact population age. Displacement-dependent replacement of contact populations is shown to cause the diagnostic evolution of friction over a characteristic sliding distance that occurs whenever slip begins or sliding conditions change.

**Key words:** Friction, fault properties, contact mechanics, state dependence, characteristic sliding distance.

## Introduction

Unstable sliding (stick-slip) is an often unwelcome phenomenon occurring in a multitude of sliding materials and mechanical systems. The scale of systems displaying unstable slip spans the range from the microscopic to that of great earthquakes having fault dimensions of a thousand kilometers or more. Extensive investigation of stick-slip in rocks has been undertaken for its possible revelance to the mechanism of crustal earthquakes and has established that rocks display somewhat complicated, but characteristic, dependence of friction on sliding history (DIETERICH, 1979, 1991; RUINA, 1993; RICE and RUINA, 1983; BLANPIED and TULLIS, 1986; TULLIS and WEEKS, 1986; GU and WONG, 1991; DIETERICH and LINKER, 1992; LINKER and DIETERICH, 1992). In addition to stick-slip, other manifestations of history- dependent frictional properties include time-dependent healing of surfaces in stationary contact, displacement weakening at the onset of slip and various transient phenomena that arise when sliding speed or normal stress change (DIETERICH, 1979, 1981; RUINA, 1983; RICE and RUINA, 1983; BLANPIED

[1] U.S. Geological Survey, 345 Middlefield Rd., MS/977, Menlo Park, CA 94015, U.S.A.

and TULLIS, 1986; TULLIS and WEEKS, 1986; GU and WONG, 1991; DIETERICH and LINKER, 1992; LINKER and DIETERICH, 1992). A slip rate- and state-depen- dent constitutive formulation, which we describe below, has found wide application for representation of these effects and for modeling of earthquake phenomena including stable creep, earthquake slip and afterslip (for example, OKUBO, 1989; DIETERICH, 1992, 1994; MARONE et al., 1991; RICE and GU, 1983; SCHOLZ, 1988; STUART, 1988; TSE and RICE, 1986).

This study shows that a diversity of materials, not limited to rocks, possesses comparable frictional properties. Although the rate- and state-dependent constitu- tive formulation furnishes an effective and unified empirical representation of laboratory observations, physical processes for the state dependence have been difficult to investigate. In this paper we summarize initial results from a technique for direct microscopic examination of sliding surfaces during slip. These experi- ments both confirm some prior concepts and provide new insights into the micromechanical processes that produce history-dependent friction effects.

### Rate- and State-dependent Friction

The usual experimental protocol for evaluating slip rate and state dependence of friction consists of changing the sliding speed in a stepwise manner under condi- tions of constant normal stress. We have found, Figure 1, that diverse materials show similar response to a change of slip speed. A step increase of slip speed results in an immediate jump in frictional resistance followed by displacement dependent decay and stabilization at a new steady-state sliding friction. The reverse is seen if slip speed is decreased. This response to changes in slip rate occurs over a wide range of temperatures, pressures and sliding rates (see, for example: BLANPIED et al., 1991; KILGORE et al., 1993). In addition to nonmetallic materials, DUPONT and DUNLAP (1993) have observed the response illustrated in Figure 1 for sliding of lubricated steel under some conditions.

A number of investigations, mentioned previously, have developed and applied slip rate- and state-dependent constitutive formulations for fault slip. This formula- tion provides a descriptive framework for the interpretation of the transient sliding phenomena illustrated in Figure 1. The following is based upon the RUINA (1983) approximation of the formulation proposed by DIETERICH (1979). The coefficient of friction may be represented by

$$\mu = \frac{\tau}{\sigma} = \mu_0 + A \ln\left(\frac{V}{V^*} + 1\right) + B \ln\left(\frac{\theta}{\theta^*} + 1\right), \tag{1}$$

where $\tau$ and $\sigma$ are shear and normal stress, respectively, $V$ is slip speed and $\theta$ is a state variable. Parameters $\mu_0$, $A$ and $B$ are experimentally determined constants and $V^*$ and $\theta^*$ are normalizing constants.
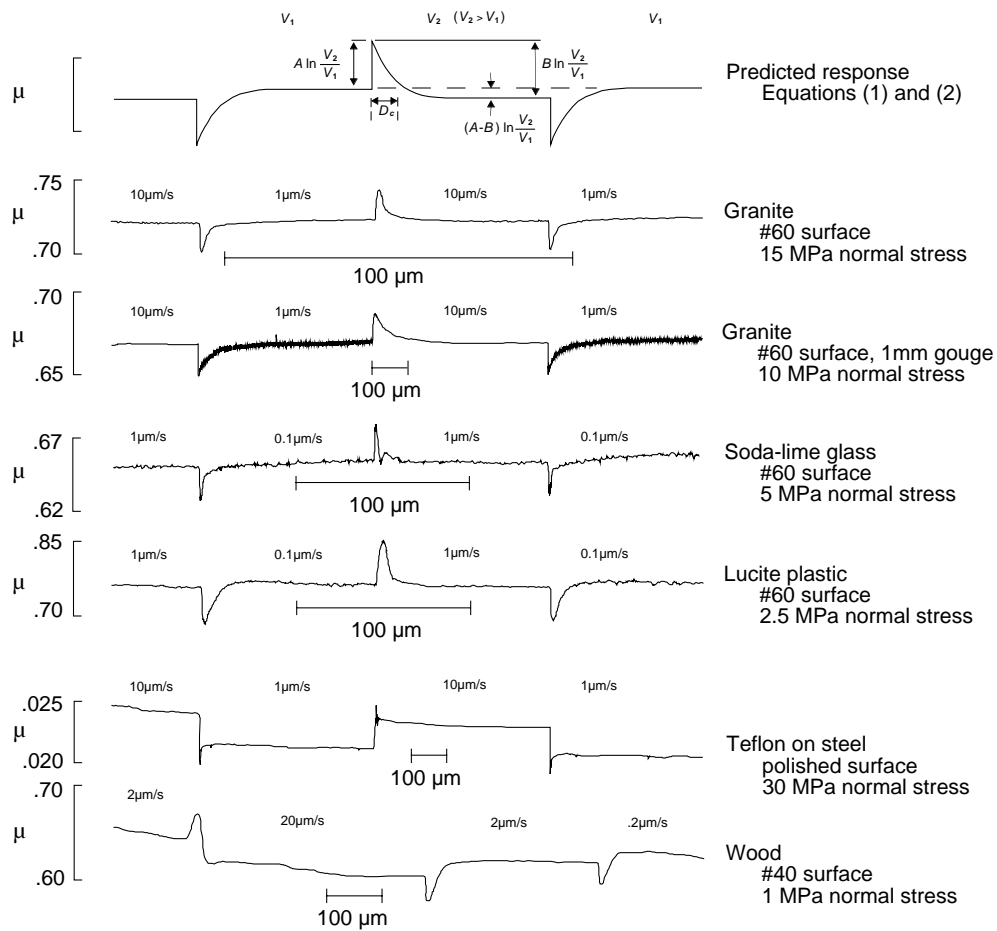
Figure 1

Effect of steps in slip speed on coefficient of friction μ in various materials. The top curve gives response predicted by constitutive equations (1) and (2). $D_c$ is commonly represented as the *e*-folding distance for change of friction following a step in slip speed. $D_c$ varies with the surface roughness and characteristics of layers of comminuted material separating the surfaces (gouge).

In an ideal velocity stepping test, parameters $A$, $B$, and $D_c$ contain the graphical interpretation indicated in Figure 1 and $\mu_0$ represents the nominal coefficient of friction which for most materials ranges from 0.5 to 0.8. In practice, it is not possible to instantaneously step to a new constant sliding speed because of finite apparatus stiffness. Apparatus stiffness effects are readily modeled (for example, TULLIS and WEEKS, 1986) and cause the rounding of friction peaks and oscillations that are visible in figure 1. With rocks, the values of the coefficients $A$ and $B$ generally vary between 0.005 and 0.015.

The characteristic sliding displacement required to stabilize friction after a change of sliding conditions is designated as $D_c$. Studies of rock friction have established that $D_c$ is approximately independent of slip speed and normal stress, but correlates with surface conditions, increasing with surface roughness and size of comminuted particles separating the sliding surfaces (for example, DIETERICH, 1979, 1981). The state variable $\theta$ acquires values determined by the recent sliding and normal stress history. A law first proposed by RUINA (1983) for evolution of $\theta$ at constant normal stress is

$$\frac{d\theta}{dt} = 1 - \frac{\theta V}{D_c}. \tag{2}$$

See LINKER and DIETERICH (1992) for discussion of alternate forms and evolution under sliding conditions of varying normal stress. Unconfirmed interpretations of equation (2) are; that $\theta$ represents a measure of the age of a continuously changing population of contacts between sliding surfaces, that the rate of change is proportional to the slip speed $V$, and that $D_c$. is proportional to the displacement required to completely change any given population of contacts (DIETERICH; 1979, 1981).

Three characteristics of this formulation are useful to the following discussion. First, if slip speed is zero, then from equation (2), $\theta$ increases by an amount equal to the elapsed time of stationary contact. Hence, from equation (1), initial resistance to renewed slip is proportional to the logarithm of contact time. This healing effect has long been recognized and linked to stick-slip instability (RABINOWICZ, 1965). Second, from equation (2), if $d\theta/dt = 0$, then the steady-state value of $\theta$ becomes $\theta_{ss} = D_c/V$. Substituting the steady-state value of $\theta$ into equation (1), and combining constants, steady-state friction can be represented as; $\mu_{ss} = \text{const} + (A - B) \ln V$. A general requirement for stick-slip is that steady-state friction decreases with increasing slip speed, or equivalently $(A - B) < 0$ (RUINA, 1983; RICE and RUINA, 1983; DIETERICH and LINKER, 1992). Third, $\theta$ evolves toward steady state over the characteristic sliding distance $D_c$. Therefore, following a change of sliding conditions, memory of prior state fades over slip distance $D_c$.

*Experiment*

Observations of regions of contact between sliding surfaces are obtained using transparent samples made from soda-lime float glass and Lucite® acrylic plastic. Both materials exhibit the full range of sliding memory effects seen in rocks and provide contrasting mechanical properties, e.g., hardness and ductility. The purpose of the observations is to investigate the origins of the state-dependent effects represented by $\theta$ and $D_c$.

Schematic representation of a sliding interface and method of observing frictional contacts are shown in Figure 2. When roughened surfaces are brought

together, contact is established only at small isolated regions and light striking the roughed surfaces of the transparent materials is scattered except at the contacts. When viewed through a microscope, contacts therefore appear as bright spots of transmitted illumination against a darker background. A similar technique for viewing surface contacts has been described (KRAGELSKII, 1965), but the method has not been previously applied to the investigation of the state-dependent effects described here.

A double shear apparatus was adopted for use in these experiments. The apparatus, described by LINKER and DIETERICH (1992), was modified using cube-shape beam turners made of optical glass, which provide an optical path through the samples normal to the sliding surfaces in addition to supporting the normal stress applied to the samples (see Figure 3). The apparatus permits servo-control of sliding speeds from $10^{-4}$ µm/s to $10^3$ µm/s at constant normal stresses to 150 MPa. Stress on the beam turners is reduced to 10 percent of the stress on the sliding surface by grinding away 90% of the original 50.0 mm x 50.0 mm roughened sliding surface leaving a small raised square button approximately 15.8 mm x 15.8 mm on each side and I mm high on the sample face. Sliding surfaces were roughened by hand lapping with # 60 or # 240 SiC abrasive and water-producing surface roughnesses heareafter referred to as coarse and fine, respectively. For the experiments reported here normal stresses varied from 1 MPa to 20 MPa and slip speeds varied from $10^{-1}$ to 10 µm/s.

The observation system employs a long working distance microscope fitted with a still camera, a high resolution monochrome (256 gray levels) video camera, and a photovoltaic silicon photodiode. The illuminating light source utilizes a focusing system matched to the microscope optics to minimize point diffraction effect and
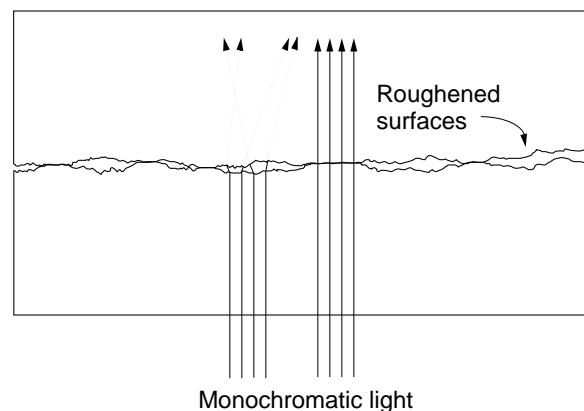


Figure 2

Schematic representation of roughened sliding surfaces. Light transmitted through the sliding blocks is scattered except at contacts.
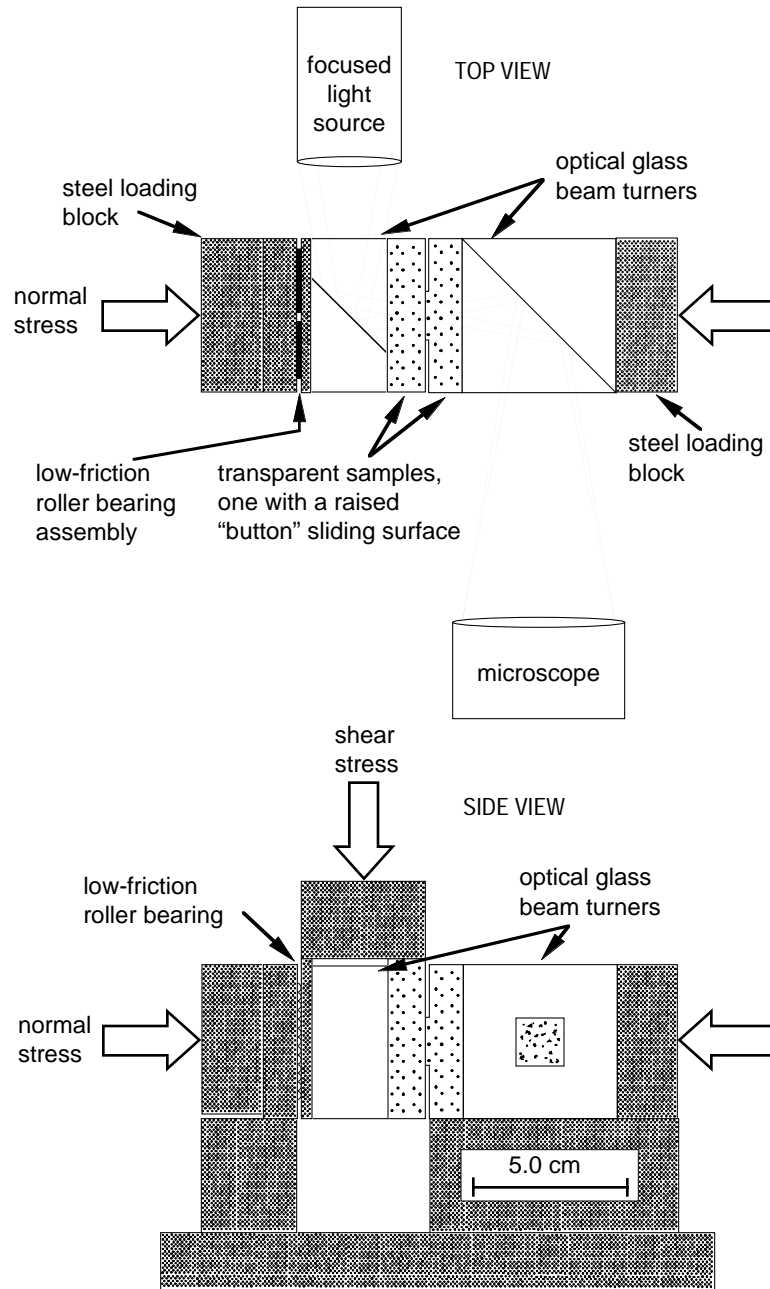
focused
light
source

TOP VIEW

optical glass
beam turners

steel loading
block

normal
stress

low-friction
roller bearing
assembly

transparent samples,
one with a raised
"button" sliding surface

steel loading
block

microscope

shear
stress

SIDE VIEW

low-friction
roller bearing

optical glass
beam turners

normal
stress

5.0 cm

Figure 3
Modified direct shear apparatus used for this study.

has a narrow bandwidth (10 nm) interference filter (550 nm center wavelength) to eliminate chromatic aberration. For direct visual observations and for photomicrographs the theoretical resolution of the optical system (1.8 μm) is attained. The resolution of digitized video images is fixed at a minimum pixel dimension of 1.9 μm.

The digitized video images are analyzed to determine both the numbers of contacts and contact areas using image processing software. This involves converting the grey level images to only black or white to distinguish areas of contact from areas not in contact. This process requires the digitized images to be inverted so that black regions represent areas of maximum light transmission (areas of contact), and white areas represent areas of minimal light transmission (areas not in contact). After comparing the digital images to direct visual observations through the microscope, a threshold grey level is determined such that all pixels lighter than this grey level are made white (no contact), and all others are made black (contact). The resultant black or white image is then easily analyzed to determine the area (number of black pixels) of each contact. From this information, statistics concerning the distribution of contact dimensions and mean contact stress were determined.

The photodiode attached to the microscope measures the intensity of the light transmitted across the sliding surfaces and provides a continuous record of total contact area that is not possible from the intermittent video images. Photodiode data were converted to relative contact area (e.g., contact area/area of sliding surface) using reference measurements of the average light intensity at points of contact and for regions not in contact. The photodiode data were converted into contact area a using the relation

$$\alpha = \frac{I - I_0}{I_{100} - I_0} , \tag{3}$$

where, $I$, is the photodiode output (volts) measured during an experiment, and $I_0$ and $I_{100}$ are measured reference photodiode outputs for equivalent contact areas of 0 and 100 percent, respectively.

Determinations of $I_0$ were made by measuring the intensity of light passing across samples resting together with no normal stress applied. Estimates of $I_{100}$ were made by determining the average intensity of light passing across several individual contacts with the samples under load. This was accomplished by analyzing an image of the sliding surface under load to determine the average grey level of the pixels in that image that defined several individual contacts. The roughened samples were then replaced with nonroughened, transparent samples in the testing apparatus. The intensity of the illumination source was then varied until the average intensity of the entire field of view of the video camera, determined by the analysis of subsequent images, matched the average intensity of the contacts. The photodiode output under these conditions is used as the value of $I_{100}$.
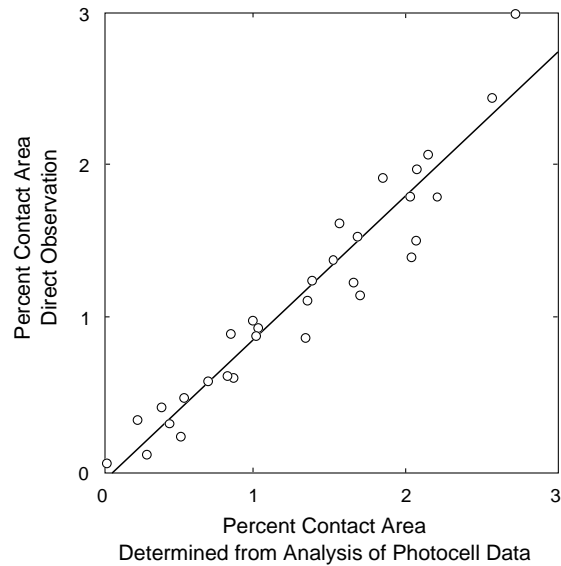
Figure 4

Contact areas determined simultaneously using the photocell method and by direct observation are given by the horizontal and vertical axes, respectively. See text for description of the methods.

Contact areas obtained from the video and photodiode data agree within the scatter of the observations (standard deviation of about ±0.0025 contact area/surface area for both methods), see Figure 4. Because the observations sample only a portion of the sliding surface, the primary source of measurement scatter appears to be from nonuniform distribution of contacts. Scatter was minimized by sampling the largest practical area for analysis and by rejecting samples which showed obviously nonuniform contact distributions. For video analysis 25-frame mosaics were obtained which represent about 11 percent of the sliding surface. Additional uncertainty arises from researcher's subjectivity in setting the threshold light intensity employed for separation of grey scale images to only black or white and from change of the background illumination as the surfaces are damaged during slip. Several refinements appear possible which should reduce these sources of scatter.

## *Results*

Photomicrographs of roughened acrylic and glass surfaces at 10 MPa normal stress are shown in Figure 5. For acrylic samples at 10 MPa applied normal stress, the distributions of the measured areas of the individual contacts have means of $45 \pm 11$ μm$^2$ and $951 \pm 181$ μm$^2$ for fine and coarse surfaces, respectively. The
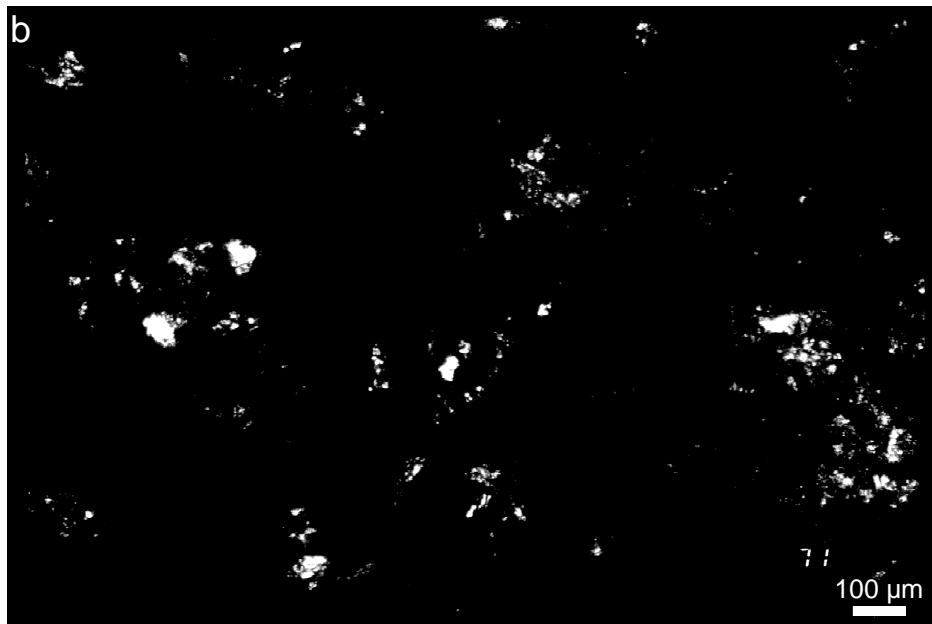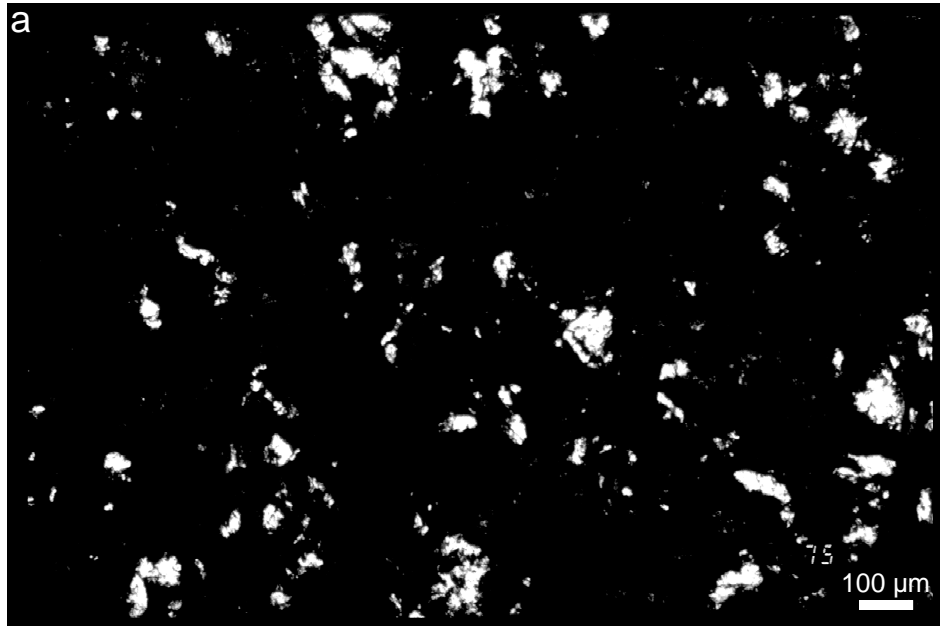
distributions of contact areas of glass at 10 MPa have means of 27 ± 2 μm$^2$ and 263 ± 66 μm$^2$ for fine and coarse surfaces, respectively.

We observe that total contact area increases linearly with applied normal stress for both the acrylic plastic and glass. Hence, average contact normal stress, obtained from the product of applied normal stress and total contact area/unit area, is independent of applied stress. In addition, we observe a linear correlation between normal stress and sliding resistance. These results conform to the usual view of unlubricated roughened surfaces which holds that friction is proportional to real area of contact which in turn is controlled by contact yielding in response to the applied normal stress. Regression analyses of the area versus applied normal stress data yield contact stresses of 399 ± 109 MPa and 5440 ± 1140 MPa for acrylic and glass, respectively which agree with the micro-indentation hardnesses of those materials. We obtained micro-indentation hardnesses of 502 ± 80 MPa and 5350 ± 300 MPa for acrylic plastic and glass, respectively., For this comparison, a 10 second time of indent was chosen as a reference. Howe However, the contact times for measurement of areas were variable and in several cases exceeded 10 seconds.
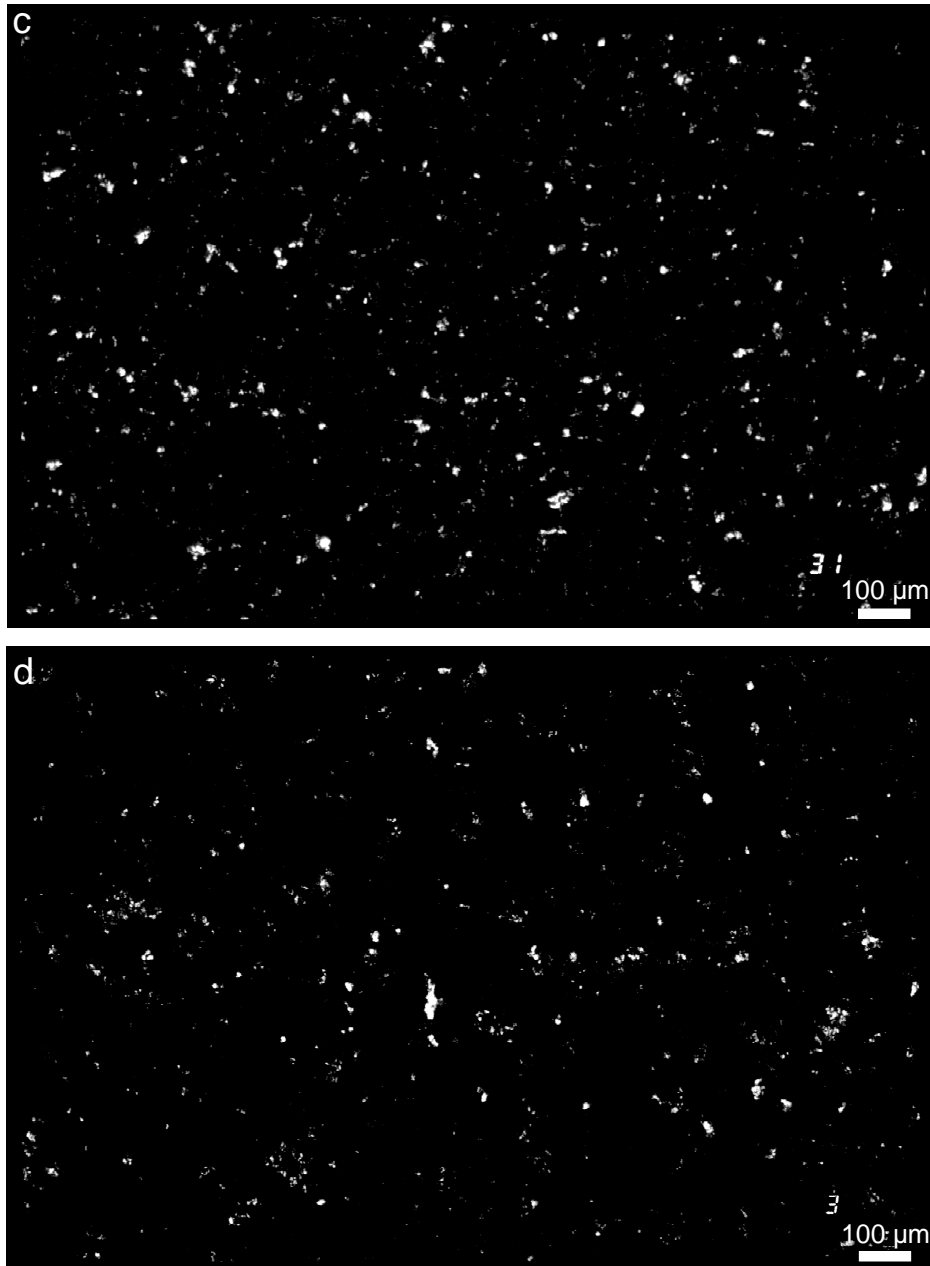
Micro-indentation hardness values were determined using a Vickers penetrator (a square-based pyramid with an included point angle of 136 degrees) made of synthetic sapphire. Load on the penetrator varied, depending on the material tested, in order to produce nominal indent dimensions of about 25 μm x 25 μm. Because the acrylic plastic undergoes significant strain hardening during the sliding tests, acrylic test surfaces were first abraded with SiC abrasive in order to approximate the near-surface deformation of the friction samples. These surfaces were then polished with # 600 wet-dry sand paper to produce a smooth surface so that the small penetrations could be easily observed and measured. Penetrations on the glass samples were made on fresh, unabraded surfaces.

Comparisons of successive video images as normal stress is increased. Figure 6a, shows that contact area increases by three processes: 1) enlargement of individual contacts, 2) coalescence of neighboring contacts and 3) appearance of new contacts. The distributions of contact sizes have the interesting property of being only weakly sensitive to normal stress, indicating that new (small) contacts appear at a rate that approximately balances the growth and coalescence of existing contacts. Details of the statistical characteristics of the contact populations and analysis of contact processes will be reported in a later paper.

Video images at increasing times of contact confirm increase of contact area with time. Figure 6b illustrates time- dependent contact growth in acrylic. The three processes observed to increase contact area with normal stress also operate to increase contact area with time (contact growth, coalescence and formation of new contacts). The time-dependent increases of area in glass are smaller than those in plastic and more difficult render in a figure. However, all three effects were also seen with the glass samples.
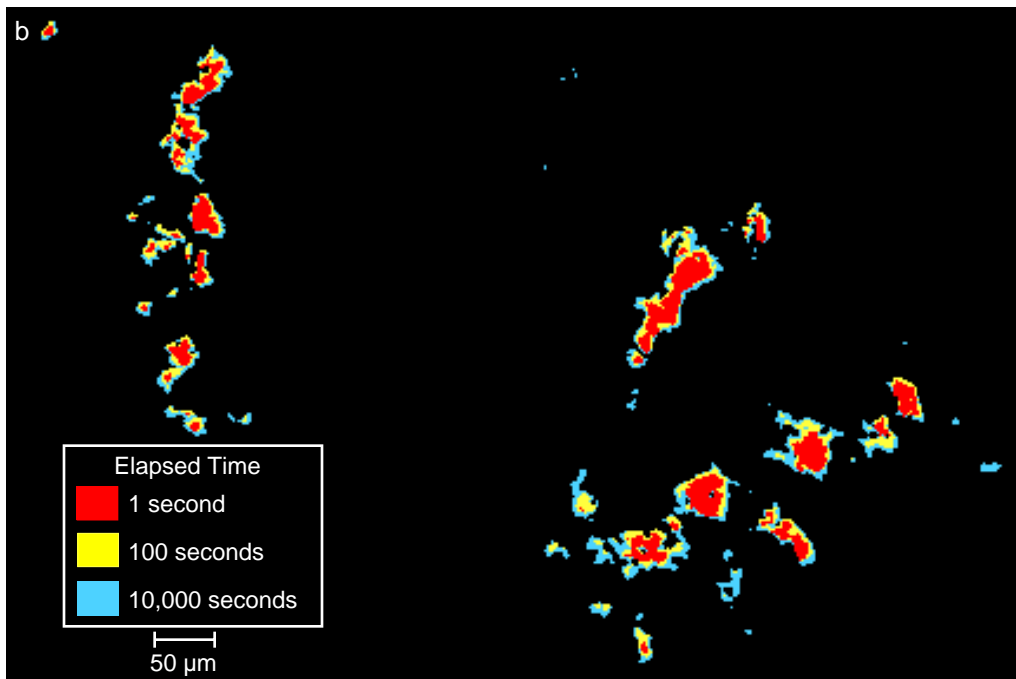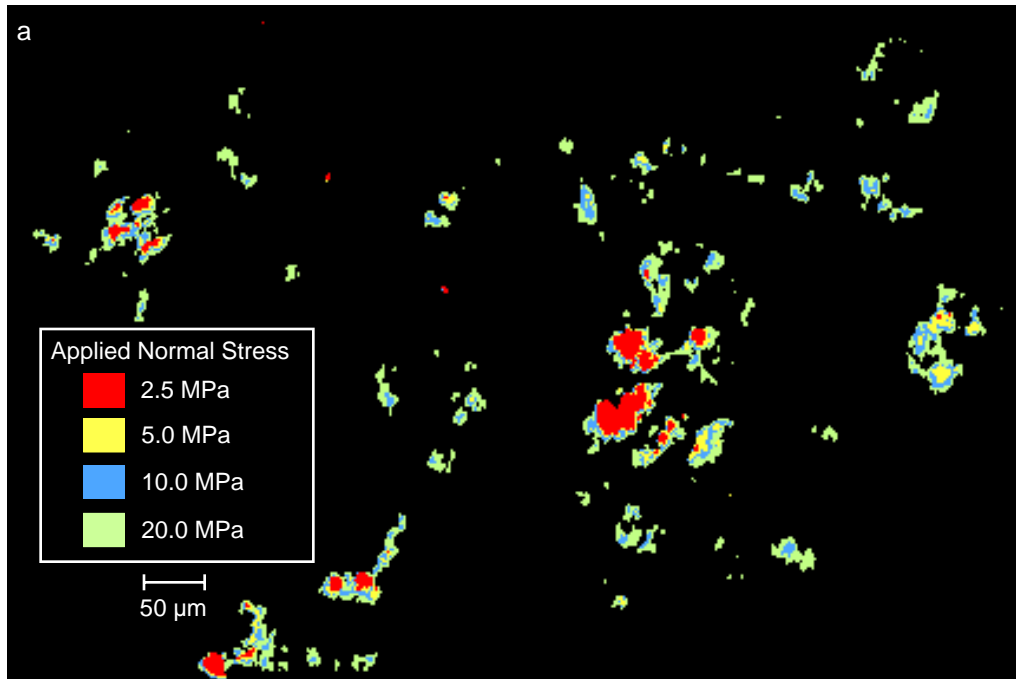
Figures 5(a), (b)

Figures 5(c), (d)

Figure 5

Photomicrographs of surfaces at 10 MPa normal stress. Contacts appear as bright spots against darker background of scattered illumination. Surfaces of acrylic plastic and soda-lime glass lapped with # 60 abrasives are shown in a) and b), respectively. Surfaces of acrylic and soda-lime glass lapped with # 240 abrasive are shown in c) and d), respectively.

Direct microscopic examination during slip shows that contacts continuously appear, change shape and disappear. Change of contact appearance during slip is smooth and continuous. Fracturing at contacts certainly occurs, particularly in the glass samples, as evidenced by extensive surface damage and abundant accumulation of finely comminuted wear particles. However, we have not observed sudden changes of contact appearance that might be indicative of unstable crack propagation or unstable contact failure. The smooth evolution of contacts, at the resolution of these observations, contradicts a commonly stated supposition that frictional slip proceeds by contact-scale stick-slip events or by unstable breakdown of contacts.

Investigation of the origins of state-dependent frictional processes included examination of contact properties during time-dependent strengthening of stationary surfaces. The experiment consists of arresting slip and holding surfaces in nominally stationary contact for some interval of time followed by renewed slip (slide-hold-slide). A transient strengthening, by the logarithm of the hold time, is observed (Figure 7). As previously described, equations (1) and (2) represent this effect as an increase of state parameter $\theta$ with the hold time. We find (Figures 6b and 7) an approximately logarithmic increase of contact area during the hold which is comparable in magnitude to the increase of indentation area observed in micro-indentation creep measurements.

In Figure 7a it is seen that peak friction does not occur at the same displacement as the peak contact area. Because of finite apparatus stiffness, some sliding takes place before the sliding speed reaches the load point speed (where friction reaches its maximum value). Once slip is initiated and contacts begin to slide past each other, the old population of larger contacts is progressively replaced by a new population of smaller contacts whose dimensions evolve over the slip distance $D_c$, to a new steady state. Therefore, the contact area measured at peak friction should be less than the peak area measured at the end of the hold period. As shown in Figure 7, the transient friction peak following a hold is comparable in magnitude to the contact area at the time of the friction peak (both normalized to their steady-state values, see Figure 7a). These observations, together with the agreement of contact stresses with indentation yield stresses, confirm that indentation creep processes affect contact area and that time-dependent increases in friction are caused by contact area creep.

During the slide-hold-slide experiments, small amounts of slip occur during a hold because the surfaces are still subjected to a shear stress. To eliminate the

Figure 6

Contact area between rough surfaces of acrylic plastic with a) increasing normal stress, and b) increasing time of stationary contact at 10 MPa normal stress. These figures were prepared by overlaying digitized video images taken at the indicated normal stresses or elapsed time of contact. Area increases by growth of existing contacts, appearance of new contacts and contact coalescence.
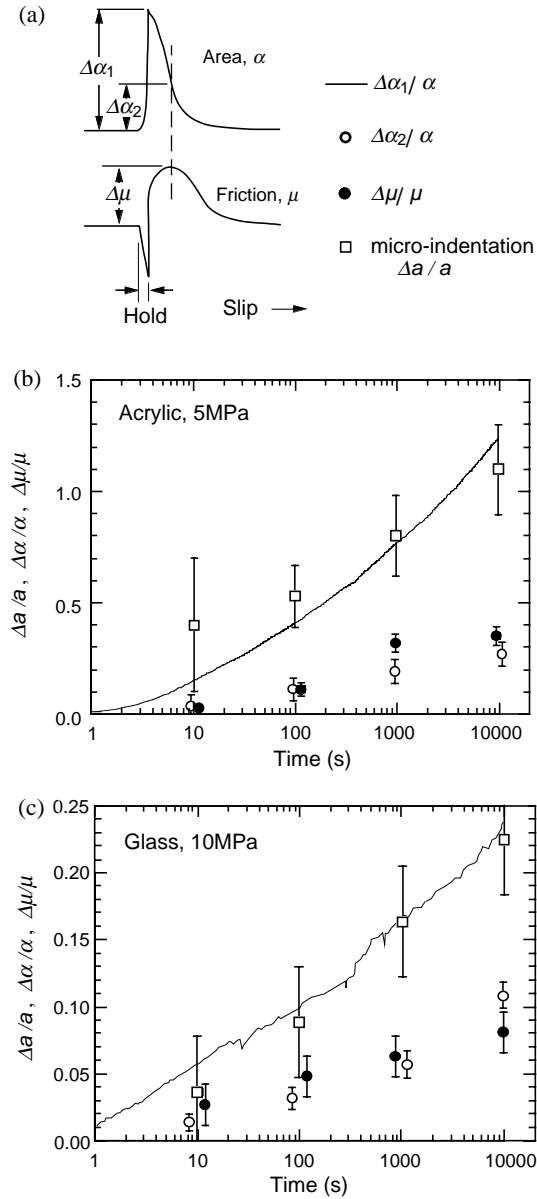
Figure 7
Normalized increases of micro-indentation area, contact area and peak friction versus logarithm of time for acrylic and glass (Figures 7b and 7c, respectively). Contact area and friction in Figure 7a are plotted against slip which has been corrected to remove the effects of finite apparatus stiffness. The contact area and friction data are normalized by $\alpha$ and $\mu$, area and friction respectively, at the start of the hold. The data for increase of indentation area with time are normalized by the 1-second indentation area $a$. Time-dependent increases of contact area measured during a hold $\Delta\alpha_1/\alpha$ (solid curve) agree with the micro-indentation area increases. Contact area measured at peak friction, $\Delta\alpha_2/\alpha$, agrees with normalized change of peak friction, $\Delta\mu/\mu$ confirming a direct dependence of friction on contact area.

possible effects of shear stress coupling during the slide-hold- slide tests, additional tests were conducted on statically loaded samples in which no shear stress was applied. These tests also yield time- dependent increases of the contact area which are consistent with the data of Figure 7. This result demonstrates a failure of a commonly employed alternate to evolution equation (2) (RICE and RUINA, 1993; TULLIS and WEEKS, 1986; LINKER and DIETERICH, 1992) that does not permit evolution of $\theta$ for stationary surfaces.

The interpretation that state dependence originates from contact creep with $\theta$ representing contact age was further examined by continuously measuring contact area during velocity stepping experiments (Figure 8). The observations establish an inverse dependence of contact area on steady-state slip speed for both acrylic and glass. Recall, from discussion of equation (2) that at steady state $\theta = D_c / V$. Hence, the inverse dependence of area on slip speed is consistent with the increase of area with $\theta$. The magnitude of the displacement dependent change of sliding resistance $\Delta\mu/\mu$ occurring after the immediate jump of friction is, from equation (1), governed solely by the evolution of the state term at the new slip speed (i.e., $\theta$ evolves from $\theta_1 = D_c / V_1$ to $\theta_2 = D_c / V_2$ at the constant slip speed $V_2$). In both materials we find that this change of friction $\Delta\mu/\mu$ following the step to the new slip speed is approximately equal to the change of contact area $\Delta\alpha/\alpha$ This result supports the interpretations of dependence of friction on contact area and control of area by population age through a process of indentation creep. From equation (2) we infer that contact population age depends on sliding history and evolves over the sliding distance $D_c$.

The parameter $D_c$ has been interpreted to be the characteristic slip required to replace a contact population representative of a previous sliding condition with a contact population created under a new sliding condition (DIETERICH, 1979, 1981). In general support of this hypothesis we find that the mean contact diameter obtained from the mean area of a contact (assuming circular contacts) is always approximately equal to $D_c$. Further support of this hypothesis is obtained from simulations of the displacement-dependent replacement of contact populations based on the analysis of digitized video images.

The simulations employ contact images, collected at some instant in a sliding experiment, to calculate the expected contact area replacement during slip subsequent to the slip when the image was recorded. It is assumed that the loss of inherited contact area occurs by contact slip. Hence, a contact of diameter $d$ is fully replaced following slip of $d$. To account for the complexity of contact geometries, we first convert the digitized grey scale video images into black and white images to define the areas of contact. We then separate the images of the individual contacts into strips, each strip one pixel wide, with the strips oriented parallel to the direction of slip along the sliding surface. The lengths of all strips are then determined. The sum of the strip lengths multiplied by an appropriate scaler gives the total contact area for that image. Following some amount of slip $d$, the loss of
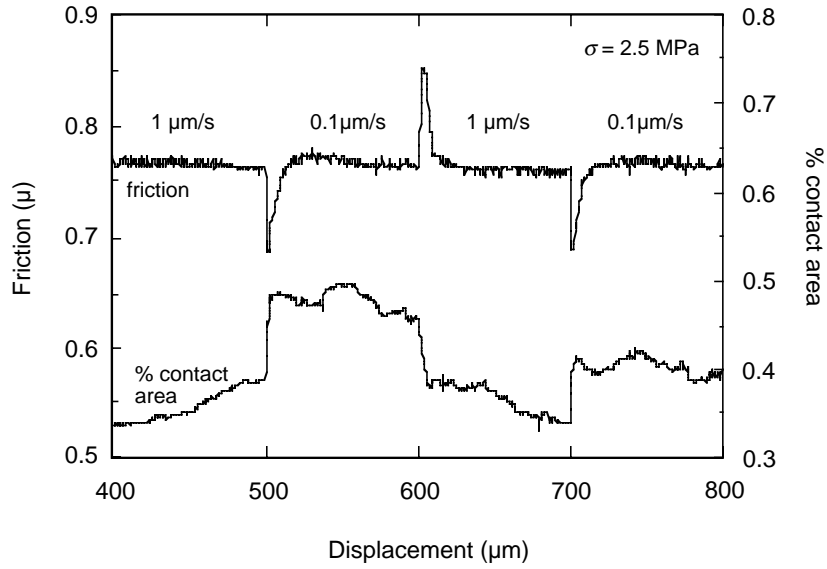
Figure 8

An example of the change of friction and change of contact area following steps of sliding speed. Normal stress is 2.5 MPa and material is acrylic plastic with surfaces roughened using # 60 abrasive.
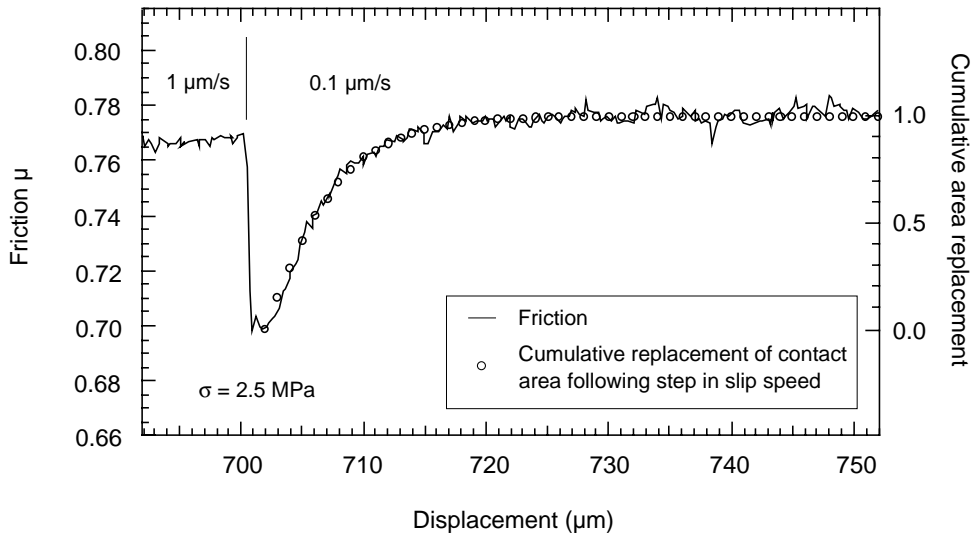


Figure 9

Displacement dependence of friction in acrylic following step in slip speed from 1 μm/s to 0.1 μm/s. Solid curve in experimental data, circles give the simulated replacement of contact area following the step in slip speed calculated from contact image data for this surface.

an inherited contact area along a strip of length $L$ is $d/L$ ($d \leq L$). The simulation proceeds in I micron displacement increments to find the cumulative area loss for each strip and from those values the net area replacement is obtained. Figure 9 compares the calculated replacement of contact area to the observed displacement-dependent evolution of friction for the same sliding surface following a jump in slip speed. These preliminary results appear to yield excellent agreement between the calculated replacement of contact area and the observed displacement-dependent evolution of friction.

## *Discussion*

A widely accepted concept of friction (RABINOWICZ, 1965; BOWDEN and TABOR, 1964), which is confirmed by our observations, holds that unlubricated friction is primarily determined by area of adhesive contacts between sliding surfaces and gives the following relation for the coefficient of frictions:

$$\mu \equiv \frac{\tau}{\sigma} = SP, \tag{4}$$

where $\tau$ and $\sigma$ are the shear and normal stress, respectively, averaged over the entire surface, $S$ is the shear strength of adhesive contacts (contact shear stress during slip) and $P$ is the inverse of contact normal stress. Contact area (per unit area of surface) is $\alpha = \tau/S = \sigma P$. For unlubricated surfaces, $S$ may approach the shear strength of the intact material. For roughened surfaces $P^{-1}$ is approximately the indentation strength of the material, indicating that $\alpha$ is controlled by yielding in response to the applied normal stress. We confirm that contact normal stress approximately equals indentation yield stress and that contact area increases with applied normal stress.

Generally, $S$ and $P$ are treated as constants. Previously, time-dependent increases of friction have been linked to the well-known indentation creep effect in which the area of indentation is found to increase approximately with the logarithm of time (BOWDEN and TABOR, 1964; DIETERICH and CONRAD, 1994). However, it has been difficult to test this relationship and alternate mechanisms relating to a time-dependent increase of the quality of constant contact areas have been proposed (RUINA, 1983; BOWDEN and TABOR, 1964). The quantitative agreement of increases of friction and contact area with the logarithm of time confirms the connection between indentation creep and the evolution of frictional state under conditions of stationary contact and suggest

$$P = P_1 + P_2 \ln\left(\frac{\theta}{\theta^*} + 1\right) \tag{5}$$

in place of constant $P$. Specifically, we interpret the state effect in friction to arise from contact area creep where state variable $\theta$ is contact population age. This interpretation is confirmed by the observation of the inverse dependence of contact area on sliding speed (see example of Figure 8) showing that equation (5) also holds during slip.

The immediate jump of friction at the time of steps in slip speed (state is constant during the jump) indicate that shear strength of contacts $S$ has a direct velocity-dependent component of the form

$$S = S_1 + S_2 \ln\left(\frac{V}{V^*} + 1\right). \tag{5}$$

We speculate that the creep mechanisms giving the rate dependence of $S$ are related to the creep mechanisms giving the time dependence of $P$. Using equations (5) and (6) in equation (4) and dropping the higher-order term gives equation (1) with

$$\mu_0 = S_1 P_1, \quad A = S_2 P_1, \quad B = S_1 P_2. \tag{7}$$

Hence, the empirical coefficients of equation (1) can be interpreted in the context of specific micro-mechanical yield and creep parameters. In view of the variety of materials found to exhibit the frictional properties represented by these formulations, it is possible that a variety of time-dependent yield mechanisms may be involved. Observations show plastic yielding generally plays a dominant role in micro-indentations on tests (for example, McClinock and Argon, 1966; Tabor, 1970; Johnson, 1985), even in nominally brittle materials (for example, Evans, 1984).

## *Conclusions*

A variety of materials have been found to exhibit complex, though characteristic, dependencies of friction on slip rate, time and sliding history that can give rise to stick-slip instability and other sliding phenomena. These properties are well represented by rate- and state-dependent constitutive formulations that have been widely applied to analysis of rock friction and for modeling of earthquake processes. We have shown that the method employed for this study provides various quantitative observations of surface contacts during slip that are of use in understanding state-dependent friction effects. This initial study employed acrylic plastic and soda-lime glass which display rate- and state-dependent friction effects and have the distinct advantages of availability and ease of sample preparation. Experiments are planned which will employ transparent minerals.

Analysis of contact size distributions and shapes shows that evolution of friction over a characteristic sliding distance $D_c$ can be attributed to the replacement of a contact population, representative of state under prior sliding conditions, with a

new contact population, representative of current sliding conditions. The characteristic sliding distance $D_c$ is a measure of the population of contact diameters. The observations demonstrate a correlation between state-dependent friction effects and indentation creep processes which tend to increase the area of contact by approximately the logarithm of contact population age. The state variable $\theta$ is a measure of contact population age. Changes of sliding resistance reflect changes of contact area and arise from shifts of contact population age. In this context the loss of strength that accompanies the onset of stick-slip instability reflects the loss of contact area that arises from the decrease of contact population age as sliding speed increases and old contacts are replaced by young contacts.

Empirical state-variable formulations have proved to be useful predictors of frictional processes including stick-slip instability. The experimental method we have employed here provides various means for relating the empirical constitutive coefficients to more fundamental micromechanical properties. However, it remains an open question to explain why materials with such diverse properties as those shown in Figure 1 should show qualitatively similar sliding history effects.

### *Acknowledgements*

### REFERENCES

BLANPIED, M. L., and TULLIS, T. E. (1986), *The Stability and Behavior of a Frictional System with a Two State Variable Constitutive Law*, Pure and Appl. Geophys. *124*, 415-444.

BLANPIED, M. L., LOCKNER, D. A., and BYERLEE, J. D. (1991), *Fault Stability Inferred from Granite Sliding Experiments at Hydrothermal Conditions, Geophys.* Res. Lett *18*, 609-612.

BOWDEN, F. B., and TABOR, D., *The Friction and Lubrication of Solids*, v. 2 (Clarendon, Oxford 1964).

DIETERICH, J. H. (1979), *Modeling of Rock Friction 1. Experimental Results and Constitutive Equations*, J. Geophys. Res. *84*, 2161-2168.

DIETERICH, J. H., *Constitutive properties of faults with simulated gouge. In Mechanical Behavior of Crustal Rocks, Geophysical Monograph 24* (eds. Carter, N. L., Friedman, M., Logan, J. M., and Stearns, D. W.) (Am. Geophys. Union, Washington, D.C. 1981) pp. 103-120.

DIETERICH, J. H. (1992), *Earthquake Nucleation of Faults with Rate- and State-dependent Strength*, Tectonophysics *211*, 115-134.

DIETERICH, J. (1994), *A Constitutive Law for Rate of Earthquake Production and its Application to Earthquake Clustering*, J. Geophys. Res. *99*, 2601-2618.

DIETERICH, J. H., and CONRAD, G. (1984), *Effect of Humidity on Time- and Velocity-dependent Friction in Rocks*, J. Geophys. Res. *89*, 4196-4202.

DIETERICH, J. H., and LINKER, M. F. (1992), *Fault Stability under Conditions of Variable Normal Stress*, Geophys. Res. Lett. *19*, 1691-1694.

DUPONT, P., and DUNLAP, E. (1993), *Friction Modeling and Control In Boundary Lubrication*, Proc. 1993 American Control Conference, San Francisco, CA, June, 1910-1914.

EVANS, B. (1984), *The Effect of Temperature and Impurity Content on Indentation Hardness of Quartz*, J. Geophys. Res. *89*, 4213-4222.

GU, Y., and WONG, T.-F. (1991), *Effects of Loading Velocity, Stiffness, and Inertia on the Dynamics of a Single Degree of Freedom Spring- slider System*, J. Geophys. Res. *96*, 21677-21691.

JOHNSON, K. L., *Contact Mechanics* (Cambridge University Press, Cambridge 1985).

KILGORE, B. D., BLANPIED, M. L., and DIETERICH, J. H. (1993), *Velocity-dependent Friction of Granite over a Wide Range of Conditions*, Geophys. Res. Lett *20*, 903-906.

KRAGELSKII, 1. V., *Friction and Wear* (Butterworths, Washington, D.C. 1965).

LINKER, M. F., and DIETERICH, J. H. (1992), *Effects of Variable Normal Stress on Rock Friction: Observations and Constitutive Equations*, J. Geophys, Res. *97*, 4923-4940.

MARONE, C. J., SCHOLZ, C. H., and BILHAM, R. (1991), *On the Mechanics of Earthquake Afterslip*, J. Geophys, Res. *96*, 8441-8452.

MCCLINTOCK, F., and ARGON, A. S., *Mechanical Behavior of Materials* (Addison-Wesley, Reading, Mass. 1966).

OKUBO, P. G. (1989), *Dynamic Rupture Modeling with Laboratory-derived Constitutive Relations*, J. Geophys. Res. *94*, 12321-12335.

RABINOWICZ, E., *Friction and Wear of Materials* (John Wiley, New York 1965).

RICE, J. R., and GU, J.-C. (1983), *Earthquake Aftereffects and Triggered Seismic Phenomena*, Pure and Appl. Geophys. *121*, 187-219.

RICE, J. R., and RUINA, A. L. (1983), *Stability of Steady-state Frictional Slipping*, J. Appl. Mech. *50*, 343-349.

RUINA, A. L. (1983), *Slip Instability and State Variable Friction Laws*, J. Geophys. Res. *88*, 10359-10370.

SCHOLZ, C. H. (1988), *The Critical Slip Distance for Seismic Faulting*, Nature *336*, 761-763.

STUART, W. D. (1988), *Forecast Model for Great Earthquakes at the Nankai Trough Subduction Zone*, Pure and Appl. Geophys. *126*, 619-641.

TABOR, D. (1970), *The Hardness of Solids*, Rev. Phys. Technol. *1*, 145-179.

TSE, S. T., and RICE, J. R. (1986), *Crustal Earthquake Instability In Relation to the Depth Variation of Frictional Slip Properties*, J. Geophys. Res. *91*, 9452-9472.

TULLIS, T. E., and WEEKS, J. D. (1986), *Constitutive Behavior and Stability of Frictional Sliding of Granite*, Pure and Appl. Geophys. *124*, 384-414.